JOURNAL OF APPLIED PHYSICS VOLUME 35, NUMBER 11 NOVEMBER 1964

Strain and Precision Lattice Parameter Measurements by the X-Ray Divergent Beam Method. I*

T. Ellis, L. F. Nanni, A. Shrier, S. Weissmann, G. E. Padawer,† and N. Hosokawa‡
Materials Research Laboratory, College of Engineering, Rutgers, The State University, New Brunswick, New Jersey

(Received 20 April 1964)

An X-ray method is described which permits a precise determination of the interplanar spacings in a crystal. The method is capable of disclosing small differences in interplanar spacings even between various sets of (*hkl*) planes of the same form and, therefore, serves as a basis for a stress–strain analysis. An error analysis of this method shows that the minimum measurable strains in the lattice, expressed as $\Delta d/d$, are a function of the diffraction angle θ. For θ varying from 35° to 65°, the minimum measurable strains vary from 0.03% to 0.009%.

A precision determination of the lattice parameter of a zone-refined tungsten crystal yielded $a_0=3.16566 \pm 0.00002$ Å. Limitations and possible applications of the method to problems in physical metallurgy and solid state physics are presented.

1. INTRODUCTION

A STRAIN analysis was recently developed by which the principal strains in a crystal can be determined provided the changes of interatomic spacings of more than six independent (*hkl*) reflections are recorded.[1] Such data are conveniently provided by the back-reflection divergent x-ray beam method. By means of this method pseudo-Kossel patterns are obtained which consist of ellipses corresponding to the reflections from a number of individual (*hkl*) planes. Changes in the interatomic spacings Δd_{hkl} induced by mechanical or chemical processes are manifested sensitively by changes in the parameters of the ellipses. By measuring the Δd values of several (*hkl*) reflections and referring them to the corresponding d spacings of the initial state, strains $\Delta d_{hkl}/d_{hkl}$ are obtained which are used as the raw data for the strain analysis.

For cubic crystals the strain analysis has been recently further developed so as to yield a complete stress–strain analysis.[2] In addition to the stress–strain configuration of the crystal, the stored elastic energy can also be measured and the magnitude and direction of the maximum shearing strain in any desired plane can be determined. Since this stress–strain analysis represents a powerful research tool for various problems in physical metallurgy and solid-state physics[1–6] and since this analysis is based on the strain data supplied by the divergent beam method, it is only fitting to inquire what precision can be obtained by this technique. This paper deals, therefore, with the new experimental developments—the precision and the advantages and limitations of the x-ray divergent beam method.

It should be clearly understood that the precision requirements for the stress–strain analysis based on the divergent beam method are much more stringent than those usually associated with conventional strain analyses based on other x-ray methods, viz., powder method. In the latter method the strains are usually obtained from extrapolated lattice parameter measurements which, of course, can also be obtained by the divergent beam method. However, if one uses extrapolation techniques in the divergent beam method for the sole purpose of obtaining a precision value for the lattice parameter, one surrenders a unique advantage which the method offers; it is an important feature of this method that each set of planes of a form in a cubic crystal gives rise to a separate ellipse. If small strains are introduced into a crystal, the size of the ellipses will change. One of them, for example, pertaining to the (*hkl*) reflection may expand, while another one, pertaining to the ($\bar{h}kl$) reflection, may contract. These changes in the dimensions of the ellipses are directly related to the changes in d spacings and the modifications of the various ellipses of {*hkl*} reflections are therefore directly related to the strain configuration of the crystal. In the powder method, on the other hand, the various (*hkl*) reflections of a form will be recorded on a single line and in the case cited above will give rise to line broadening and thus to the usual complications associated with this effect.

Since the experimental differentiation between various (*hkl*) planes of a form is fundamental for an effective stress–strain analysis, this paper will be principally concerned with the precision that can be obtained from measurements of the interatomic spacings of a number of {*hkl*} forms. In addition to this investigation of strain measurements, a complete analysis of precision lattice parameter measurements will also be offered.

* This work was sponsored by the Aeronautical Systems Division, U. S. Air Force Systems Command, Wright-Patterson Air Force Base, Ohio, under contract AF33(657)-10872.

† Present address: Massachusetts Institute of Technology, Cambridge, Massachusetts.

‡ Present address: University of Osaka Prefecture, Sakai, Japan.

[1] T. Imura, S. Weissmann, and J. J. Slade, Acta Cryst. 8, 786 (1962).

[2] J. J. Slade, S. Weissmann, K. Nakajima, and M. Hirabayashi, J. Appl. Phys. 35, 3373 (1964) (following paper).

[3] S. Weissmann, T. Imura, K. Nakajima, and S. E. Wisnewski, J. Phys. Soc. Japan 18, Suppl. III, 179 (1963).

[4] S. Weissmann and N. Hosokawa, J. Australian Inst. Metals 8, 25 (1963); *ibid.*, p. 377.

[5] M. Hirabayashi and S. Weissmann, Acta Met. 10, 25 (1962).

[6] S. Weissmann and K. Nakajima, J. Appl. Phys. 34, 611 (1963).

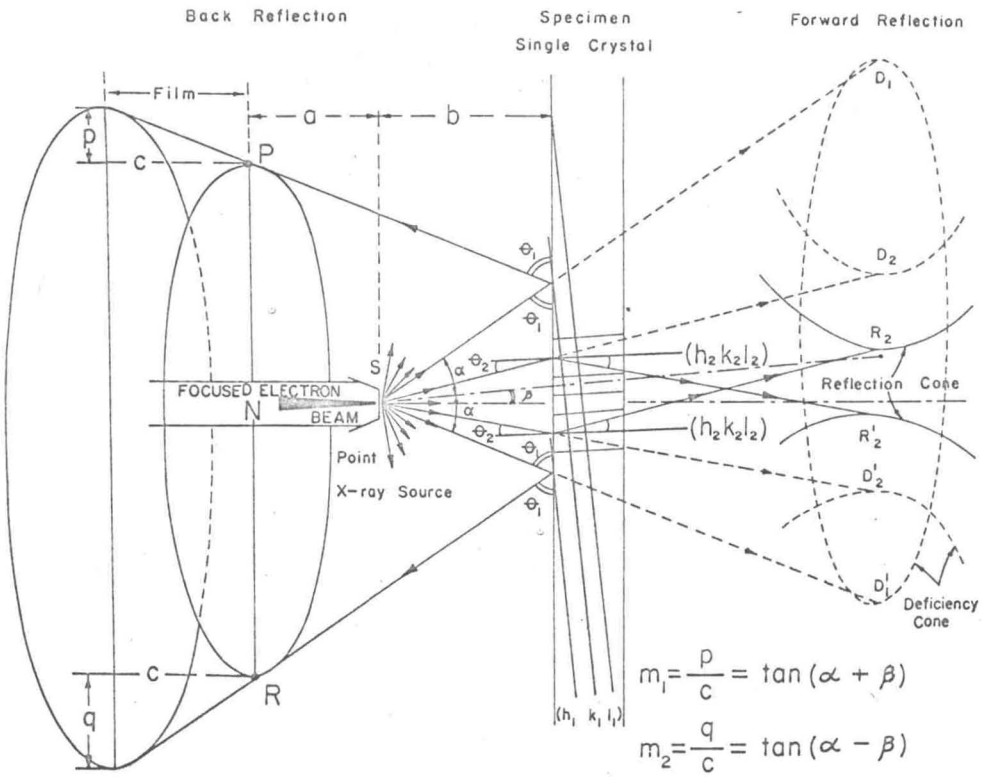

FIG. 1. Schematic representation of the generation of pseudo-Kossel patterns by the divergent beam method.

2. DESCRIPTION OF METHOD

The divergent beam method utilizes a long, horizontal ray tube, shown schematically in Fig. 1. An electron am originating from an electron gun is focused by ans of an electromagnetic lens onto the tip of the num-tight tube closed by a thin metal foil.[7] Since metal foil is bombarded by the electron beam, it ctions as an x-ray target. By operating the tube at a table voltage, an x-ray beam composed mainly of aracteristic radiation emerges from the tip of the tube, hibiting a divergence of nearly 180°. At the point of ergence the beam size is about 10 μ in diameter. When beam impinges on the specimen, which is placed at stance of 0.4–3 mm from the tip of the tube, diffrac- patterns of the characteristic spectrum in trans- sion as well as in the back-reflection region may be orded. We shall be principally concerned with the alysis of the back-reflection patterns, since these can obtained conveniently even from thick specimens, exposure time for a tungsten crystal being only sec. The technique of measuring the back-reflection ttern, which will be subsequently described in detail, with some slight modification, equally applicable to smission patterns.

The divergent beam patterns are analogous to the known Kossel patterns, except that the former are produced by an x-ray source located outside instead of inside the crystal. Therefore, we refer to them as pseudo-Kossel patterns.

The diffraction cones intersect the film in ellipse-like figures (Figs. 1 and 2); and although these figures, strictly speaking, represent curves of higher orders, we shall refer to them as ellipses.

Each ellipse corresponds to a reflection from a definite (*hkl*) set of planes, the *d* spacing of which can be ac-

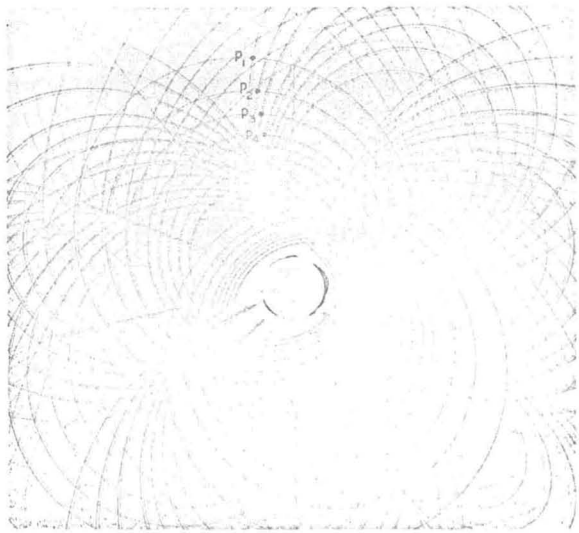

FIG. 2. Multiple exposure photograph of tungsten single crystal.

[7] An x-ray tube of this type and a diffraction unit ("Microflex") commercially produced by the Rigaku-Denki Company, Tokyo, Japan.

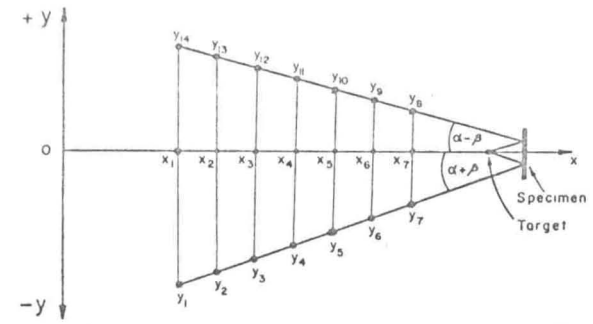

FIG. 3. Schematic representation of multiple exposure technique.

curately determined from measurements of the parameters of the corresponding ellipse.

It was found that the measurements of the film and specimen distance from the x-ray source constitute the principal source of error. These distances are shown in Fig. 1 as a and b, respectively. To eliminate this and other error sources, a number of innovations in experimental and measuring techniques were introduced which will be described presently.

It may be seen from Fig. 1 that the following direct relationship can be established between α, β and the slopes m_1, m_2 of the diffracted rays:

$$m_1 = p/c = \tan(\alpha+\beta), \tag{1}$$

$$m_2 = q/c = \tan(\alpha-\beta), \tag{2}$$

where α is the semiapex angle of the incident x-ray cone equal to $\pi/2-\theta$, θ being the Bragg angle, and β is the angle subtended by the normal of the reflecting (hkl) plane and the axis of the x-ray tube. $c=x_1-x_2$ is the distance between two consecutive film positions (Fig. 3).

If the slope parameters m_1 and m_2 of an (hkl) reflection are experimentally determined, one obtains the value of α and therefore the corresponding value of the Bragg angle θ from the solution of Eqs. (1) and (2). Subsequent substitution in the Bragg equation yields the corresponding d value.

The determination of the d spacing of an (hkl) set of planes is thus independent of the troublesome a and b parameters if the slopes m_1 and m_2 of the diffracted rays can be obtained. The principal innovation consists, therefore, of a precision determination of the slopes by a method of least squares employing a multiple exposure technique and exact measurements of distances between consecutive film positions. This is accomplished through the use of precision spacers. Thus in this method the film, after being exposed once, is moved a known distance (x_1-x_2) and a second exposure is taken. After repeating this procedure seven or eight times the film is processed in the usual way. Consequently, instead of a single ellipse, one obtains a pattern consisting of a family of seven or eight ellipses corresponding to one (hkl) reflection. Figure 2 represents such a multiple exposure diagram of an undeformed, zone-refined tungsten crystal in which the elliptical patterns have been recorded at eight different film positions (x_1 to x_8).

Figure 3 shows schematically the multiple exposure method. The points y_8 and y_7 are the intersections of the major axis with the ellipse produced during the first exposure and x_7 is the distance of the film from a fixed origin 0. Similarly, y_9 and y_6 are the intersections with the second ellipse and x_6 is the corresponding film distance, and so on.

If the equation to the line y_1y_7 is

$$y = m_1x + B_1,$$

one obtains by means of the least-squares method (see Appendix A)

$$m_1 = \sum y_i(x_i-\bar{x})/\sum(x_i-\bar{x})^2, \quad i=1, 2, 3\cdots 7.$$

But the slope of this line is also tan $(\alpha+\beta)$, and

$$Km_1 = \tan(\alpha+\beta), \tag{3}$$

where K is the film shrinkage factor.

Similarly for the line $y_{14}y_8$,

$$Km_2 = \tan(\alpha-\beta). \tag{4}$$

By combining Eqs. (3) and (4),

$$\alpha = \tfrac{1}{2}[\arctan(Km_1)+\arctan(Km_2)]. \tag{5}$$

Also $\theta=\pi/2-\alpha$. Therefore

$$d = \lambda/2\cos\alpha. \tag{6}$$

3. EXPERIMENTAL TECHNIQUE

The precision measurements of the d spacings and lattice parameters by the divergent beam method depend on a number of factors which must be closely controlled and which will be presently discussed.

a. Film Measurements

It has been shown that the precision of the d values is greatly dependent on the accuracy of the slope parameters m_1 and m_2, which in turn depend on the accuracy of measurements of the y_n ordinates and x_n abscissas of the multiple exposure diagram (Fig. 3).

The y_n coordinates are measured along the major axis of the ellipse corresponding to a specific (hkl) reflection, this axis being extended through the entire family of ellipses generated by the multiple exposure technique. Before the major axis can be constructed it is necessary to determine the center of the film. If the points of intersection of two families of ellipses p_1, p_2 etc. are connected, a line is produced which extrapolates through the center of the film (Fig. 2). If this process is repeated for a number of intersections, it is possible to locate this center accurately. Once it has been located, a major axis is constructed on the film with the aid of precision dividers. The actual readings of the y_n

ordinates are carried out with the aid of an automatic ording microphotometer (Rigaku-Denki MP-3). The e profiles of the various ellipses of a family are traced t along the major axis and the peak-to-peak distances the profiles, measured with an accuracy of $\pm 5\,\mu$, de- e the end-points of the corresponding y_n coordinates.

The x_n coordinates are controlled by fixed precision pacers which define the discrete film positions and hich span the range of specimen-to-film distance from 5 mm down to virtually zero. The size of the ellipses hich can be recorded is limited by the dimensions of he film and the existence of a hole at its center. Therefore, the selection of the discrete film positions will be overned by considerations pertaining to the completion f the elliptical patterns. For large values of y_n some ortions of the ellipses may fall outside the film area and onsequently the selection of x_n will depend principally n crystal orientation, wavelength used, and lattice pacing of planes which are being measured.

To insure accurate determinations of the x_n coordinates it is necessary to satisfy two requirements: (1) the lm should be perfectly flat and (2) the film surface hould be maintained normal to the direction of its displacement. The first requirement was fulfilled by achining grooves in the backplate of the film cassette so that a vacuum could be applied. Only when the film ad been flatly pressed to the backplate through the pplication of the vacuum was the clamping frame ghtened. The second requirement is satisfied by accurate machining of the cassette. Special care must be aken in mating the cassette base with the spacers to educe errors in the determination of the discrete film ositions x_n.

It was observed that the precision of measurements of the d spacings increases with decreasing α, that is, with ecreasing θ values. Consequently, it is highly desirable o record a great many complete ellipses in the vicinity f the center of the film. To minimize the interception f the diffracted x rays at small α values by the x-ray be itself, a long, tapered tip was fitted to the tube. his tip may be described as a truncated cone having a emiapex angle of 7°, a circular tip surface of 0.16-cm 16-in.) diameter and a height of 4.45 cm (1.75 in.)

b. Photographic Technique

A number of precautions in photographic processing ave to be taken to achieve a high degree of precision. s, for example, absolutely imperative that the film rinkage be uniform (isotropic) if the differences in pacings between various (*hkl*) reflections of a single m are to be utilized as a basis for a subsequent strain alysis After long experimentation it was found that Pont Cronar base, single-coated, graphic arts film 8×12 in.) satisfied the requirements for isotropic film rinkage. Correction for film shrinkage is made by pressing a standard scale on the exposed film and easuring it after photographic processing.

In order to minimize film shrinkage and background scattering, and thereby produce maximum contrast, the following photographic processing practice was adopted. All the films were developed for 2 min in Kodak HC110 developer diluted 5:1, followed by fixing in Kodak x-ray fixer for 6 min. Washing for six minutes and then immersion in Photoflo solution for 30 sec was followed by natural drying of the film. In this way it was possible to reduce film shrinkage to a minimum and also to insure that any dimensional change was uniform over the whole film.

c. Computer Programming

A computer program was written to expedite the repeated computation of d spacings. The input to this program was: coordinates (x_i, y_i), shrinkage factor, and wavelength used. The output was: d spacings and their corresponding standard errors.

In addition, a program was also written for the computation of the lattice parameter based on the method of weighted least squares. The input to this program was: d spacings, standard error of d spacings, and Miller indices of planes. The output was: the parameters of the weighted least-squares line and their associated standard errors. Mathematical details for the computation of the d spacings, lattice parameter, and respective errors are given in Appendix A.

The output of d-spacing computations was used for the computation of the stress–strain configuration of the strained crystals.[1,2] Indeed, it is primarily for reasons of attaining the highest degree of precision in the stress–strain analysis of crystals that the precision measurements by the divergent beam method were developed here in such detail.

4. EFFECT OF HOMOGENEOUS AND INHOMOGENEOUS STRAINS ON THE PSEUDO-KOSSEL PATTERN

If the crystal is subjected to long-range elastic strains or to homogeneous internal strains (residual strains), the shape of the pseudo-Kossel lines will be significantly altered. The homogeneous strains are then manifested by changes in the length of the major axis of the elliptical patterns. These changes in turn affect the slope parameters m_1 and m_2 and consequently the strain fluctuation can be recorded in terms of the changes of the d spacings of various (*hkl*) planes. Thus, if the changes of d spacings of more than six independent (*hkl*) planes are recorded, the complete strain distribution of the crystal can be obtained.[1,2] However, if the strains are inhomogeneous, then in addition to dimensional changes of the elliptical pattern local line broadening, kinking or displacement of line segments will occur. The effect of such strains on the pseudo-Kossel lines is shown in Fig. 4. From the schematic drawing of Fig. 1 it may be seen that adjacent areas on the specimen surface give rise to adjacent segments of

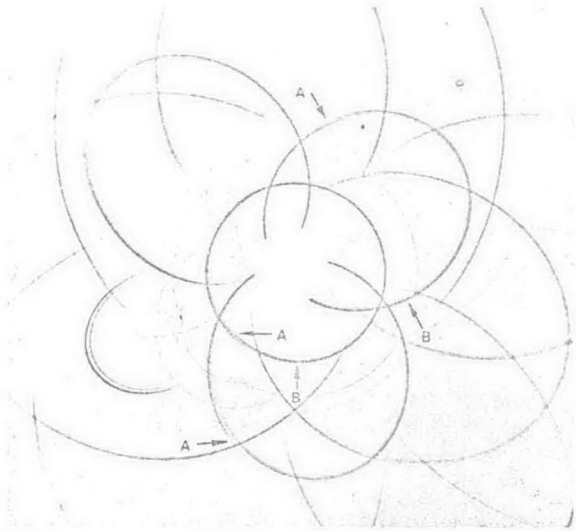

FIG. 4. Single exposure photograph of deformed tungsten crystal. Local lattice misorientation at A and line broadening at B give evidence of inhomogeneous strains.

the elliptical pattern. Consequently, the kinking and the displacement of line segments are directly associated with local lattice misorientation. This misorientation can be determined when the specimen-to-film distance, the displacement of the line segments, and their respective distances from the center of the film are known. The divergent beam method may, therefore, also be viewed as an x-ray topography method. The most precise measurements are obtained from reflections with large θ values, permitting one to detect lattice misorientations as small as 0.05°.

Local line broadening, indicated by arrows in Fig. 4, is a manifestation of inhomogeneous strains. If such line broadening occurs, the strain analysis can be extended to include intensity studies of the line profile. These are carried out by means of a microdensitometric tracing of the line profile across the broadened region. The intensity data thus obtained serve as the basis of a Fourier transform analysis.[8]

5. INCOMPLETE ELLIPSES

The crystallographic orientation of the reflecting specimen surface and its distance from the target are generally chosen so that a number of complete ellipses appear on the film. In some cases, however, extraneous crystallographic considerations predetermine the orientation of specimen faces. Some, or even most of the ellipses may then be incomplete; parts of them may fall within the central hole of the film or be blocked out by the shadow of the target. Such ellipses cannot be used for the computation of d spacings by the methods previously described. The decrease in the number of measurable d spacings, in turn, impairs the accuracy of the strain analysis, or even (if it falls below six) renders it impossible. The difficulty may be circumvented by the use of a composite target emitting two different characteristic wavelengths. Such a target has been produced, for instance, by using an iron foil plated with cobalt. The radiation emitted contains in this case CoK_α and FeK_α. It is convenient, though not necessary, that the intensities of the two characteristic radiations be made approximately equal by a suitable choice of the plating thickness. Two superimposed exposures at different film-to-specimen distances are required and the film shift between the two exposures must be known precisely. Figure 5 is a pattern of incomplete ellipses produced in this manner with a composite target.

The method of computation of d spacings is given in Appendix B.

6. RESULTS

As anticipated, no significant difference in d values among the various (hkl) planes of a form was found in the unstrained tungsten crystal. Therefore, for each $\{hkl\}$ form investigated, the average d value $\bar{d}$ was determined and these values are listed in Table I.

It will be recalled that the d spacing is obtained from α by Eq. (5) and that α in turn is obtained from the slope parameters m_1 and m_2 by Eqs. (3) and (4). The standard errors of the slopes introduced by the physical measurements results in standard errors of α which in turn propagate as standard errors of d. The average of this standard error in d for each $\{hkl\}$ form, denoted by $\bar{\sigma}_d$, was determined and is also listed in Table I. Details concerning the calculation of the propagation of errors are discussed in Appendix A.

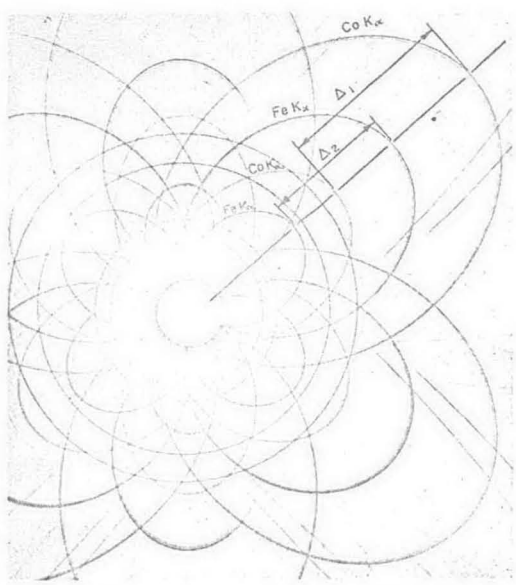

FIG. 5. Double exposure photograph of Ni–25% Fe single crystal. FeK and CoK radiations were employed for analysis of incomplete pattern.

[8] J. J. Slade in Conf. VI Intern. Union of Crystallographers, Rome, September, 1963 [Acta Cryst. 16, A104 (1963)].

TABLE I. Summary of error analysis of x-ray divergent beam method using an as-grown, zone-refined tungsten single crystal.

$\{hkl\}$	{321}	{222}	{310}	{220}	{211}
No. of observations	24	15	28	11	7
$\bar{d}$	0.84601	0.91381	1.00085	1.11912	1.29230
$\bar{\sigma}_d$	0.00008	0.00026	0.00029	0.00036	0.00039
$\bar{\sigma}_d/\bar{d}$, %	0.009	0.028	0.029	0.032	0.030
σ_d^*	0.00016	0.00028	0.00061	0.00076	0.00083
$1/\sigma_d^{*2}$	4.0829×10^7	1.2958×10^7	0.2675×10^7	0.1740×10^7	0.1254×10^7
a'	3.16547	3.16561	3.16496	3.16534	3.16549
$\bar{\theta}$	65.57	57.45	50.32	43.49	36.59

It should be understood that the σ_d values from which $\bar{\sigma}_d$ was obtained are a measure of the precision of the technique, that is, they express the experimental error in each measurement of d spacing. The $\bar{\sigma}_d$ should be compared to the σ_d^* values listed in row 6 of Table I which are the standard deviations of d spacings of the $\{hkl\}$ forms. σ_d^* measures, therefore, more than the experimental error and its physical significance seems to be intimately related to the residual strain distribution in the as-grown crystal. It will be noted from Fig. 6 that both $\bar{\sigma}_d$ and σ_d^* decrease with increasing Bragg angle θ and that for all $\{hkl\}$ forms, excepting {222}, the σ_d^* are nearly twice as large as the corresponding $\bar{\sigma}_d$ values.

The precision determination of the lattice parameter a_0 was carried out by adopting a sequence of steps which will be outlined presently.

(1) It may be seen from Table I that a considerable number of determinations of d spacings has been carried out for each $\{hkl\}$ form investigated. From each d value of an $\{hkl\}$ form, the lattice parameter a' was computed using the relation $a'=d\cdot(h^2+k^2+l^2)^{\frac{1}{2}}$.

(2) To each a' of an $\{hkl\}$ form thus obtained a value of the Nelson–Riley function, $\frac{1}{2}[(\cos^2\theta/\sin\theta)+\cos^2\theta/\theta]$, was assigned. The θ value used for this computation corresponded to the d spacing from which each a' was originally derived.

(3) Since the error in the computation of d and therefore the error in a' diminishes with increasing θ (Fig. 6), a statistical weight was assigned to each a' which is proportional to $1/(\sigma_d^*)^2$ (see Appendix A).

(4) Employing a method of least squares, the lattice parameter a_0 was obtained by extrapolation of the Nelson–Riley plot of the weighted a' values. The slope of this least-squares line is then given by

$$b=\sum n_i w_i a_i'(x_i-\bar{x})/\sum n_i w_i(x_i-\bar{x})^2$$

and the y intercept by

$$a_0=(\sum w_i a_i'/\sum w_i)-b\sum x_i w_i/\sum w_i,$$

where $x_i=\frac{1}{2}[(\cos^2\theta_i/\sin\theta_i)+\cos^2\theta_i/\theta_i]$ (the value of the Nelson–Riley function), $w_i=[1/(\sigma_{d_i}^*)^2]/[\sum 1/(\sigma_{d_i}^*)^2]$ (the statistical weights), $\bar{x}=\sum n_i w_i x_i/\sum n_i w_i$.

The following results were obtained:

$$b=-3.88\times10^{-4}\pm0.56\times10^{-4}$$
$$a_0=3.16554\pm0.00002\text{ Å}.$$

The lattice parameter a_0 was corrected for refraction by adding to it a term $a_0(1-n)$, where n is the coefficient of refraction.[9] For tungsten and using CuK_{α_1} radiation ($\lambda=1.54051$ Å) the correction factor for refraction was 157×10^{-6} Å. Since the ambient temperature during the experiments was 28°C, a temperature correction was also applied[9] using the expression

$$a_2=a_1+\alpha a_1(T_2-T_1),$$

where a_1 and a_2 are the lattice parameters at temperatures $T_1=28$°C and $T_2=25$°C, respectively, and α, the coefficient of expansion of tungsten, is 4.6×10^{-6} °C^{-1}. With these corrections applied the lattice parameter a_0 is 3.16566 Å at 25°C.

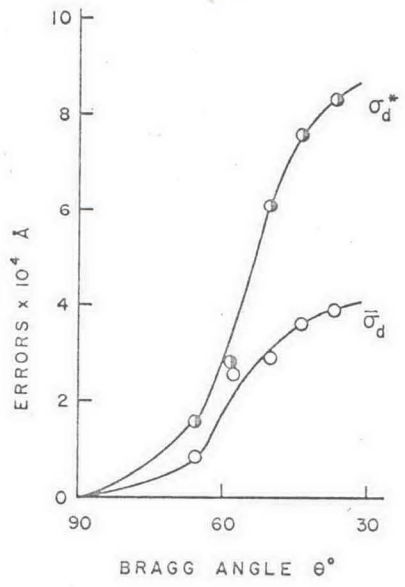

FIG. 6. Dependence of the d-spacing errors on the Bragg angle.

[9] *International Tables for X-Ray Crystallography* (Kynoch Press, England), Vol. 3.

7. DISCUSSION OF RESULTS

The newly developed stress–strain analysis[1,2] is based on the ability of the divergent beam method to record sensitively the strains in a crystal in terms of the changes of d spacings of the various (hkl) reflections. The question that arises is: What is the precision of strain measurement that can be obtained by the divergent beam method?

It is quite evident that the strains $(\Delta d/d)$ smaller than the experimental error in d spacing, given by $\bar{\sigma}_d$, cannot be measured. Focusing our attention on Table I and Fig. 6, we note that $\bar{\sigma}_d$ is a function of the Bragg angle θ, declining with increasing θ. It can be seen that for planes belonging to the {211} form in tungsten crystals, the minimum value of $\bar{\sigma}_d$ is 0.00039 Å and, therefore, strains smaller than 0.030% (=0.00039/1.29230) cannot be measured. For the {321} form the precision improves to 0.009% strain. It follows from the dependence of $\bar{\sigma}_d$ on θ that if small strain variations are to be measured for a given crystal orientation, the radiation used should be such as to yield the maximum number of ellipses in the vicinity of the center of the film.

For the successful application of the stress–strain analysis it appears useful to construct at the outset a curve such as that shown in Fig. 6, which defines the limits of the largest experimental error, namely, that of $\bar{\sigma}_d$. It is significant that in this error analysis the σ_d* values which represent the standard deviations of the d spacings of the $\{hkl\}$ forms turned out to be nearly twice as large as the corresponding experimental errors $\bar{\sigma}_d$. This difference between σ_d* and $\bar{\sigma}_d$ is interpreted to be due to small residual strains which the divergent beam method seems to be capable of detecting even in as-grown, zone-refined crystals.

The decline of σ_d* and $\bar{\sigma}_d$ with increasing θ is due to a number of factors that are common to all diffraction methods in which the highest precision of measurements is obtained from lines with the largest diffraction angles. They need not be discussed here. One factor, however, is peculiar to the divergent beam method and arises from the method of measurement of the diffraction profiles. As the α value of the reflecting (hkl) planes increases (decreasing θ), the recorded ellipses are further removed from the center of the film. The decrease in the angle between the diffracted rays and the film causes an increase in the width of the recorded line. Since this line broadening results in a flattening of the diffraction maximum, an error in measurement is introduced, due to the increased uncertainty of the exact peak-to-peak distance of the line profiles.

It is interesting to compare the results of our precision lattice parameter measurement with the results obtained from an international project conducted by the International Union of Crystallographers Commission on Crystallographic Apparatus.[10] The result of the present investigation for tungsten is $a_0=3.16566 \pm 0.00002$ Å (the standard error of the mean based on 85 observations), whereas the average value obtained from the International Union of Crystallographers project, in which 16 laboratories participated, was $a_0=3.16522 \pm 0.00009$ Å.

The difference of 0.0004 Å between the values of the lattice parameter can be satisfactorily explained if one considers the impurity content of the samples studied. The material used in this investigation was a zone-refined crystal containing virtually no substitutional impurity atoms and having 2 ppm oxygen, 9 ppm carbon, 4 ppm nitrogen. On the other hand, the sample studied by the International Union of Crystallographers Commission was a polycrystalline specimen of 99.27% to 99.92% purity. Optical spectrographic examination showed small amounts of Ca, Mg, Si, B, and Cr. A wet chemical analysis showed 0.19% Fe_2O_3 and 0.06% SiO_2.[10] Substitution of W atoms by the impurities in concentrations such as these would give rise to a decrease of the lattice parameter and bring the value of a_0 published by the International Union of Crystallographers very close to that found in the present investigation.

8. APPLICATIONS AND LIMITATIONS OF THE METHOD

The stress–strain analysis based on the divergent beam method has already been applied to a number of problems in physical metallurgy and solid state physics. In all these problems the aim was to obtain quantitative information about the structural changes induced by lattice defects insofar as they manifest themselves by the concomitant changes in the strain distribution. Thus the method has been applied to the analysis of the strain distribution in the age-hardening of an Al–3.85% Cu crystal.[1] It was also applied to the study of ordering in the Cu–50% Au alloy,[2] where tetragonality strains induced by the ordering process have been analyzed by this method.

The divergent beam method becomes a particularly powerful research tool when correlated with the study of lattice defects by transmission electron microscopy.[2,3,6] As practiced in this laboratory, the single-crystal specimen is first studied by the x-ray method to obtain the stress–strain configuration. Subsequently the specimen is thinned down and viewed by transmission electron microscopy.

This combination of methods was also employed in the study of neutron-irradiated quartz when the change in strain distribution was analyzed as a function of radiation dosage[3,6] and in the study of the yield phenomena of refractory metal crystals where the slip activity in the pre-yield, microstrain region was explored.[4] It is currently applied in such diversified investigations as the study of the strain distribution

[10] W. Parrish, Acta Cryst. 13, 838 (1960).

associated with magnetic anisotropy, dispersion hardening, ductile–brittle transition of refractory metals and solution hardening in alloy single crystals.

If desired, the target of the x-ray tube may consist of an alloy, in which case the diffraction pattern recorded on the film will consist of ellipses characteristic of the elements of the target material.[1] Consequently, precision measurements can be carried out as a function of different wavelengths under identical photographic processing conditions. If the alloy of the target material contains elements of high and low atomic number, strain measurements can be carried out on the specimen which may be made a function of the depth of penetration of the corresponding radiation. This aspect may turn out to be particularly useful for a number of problems in physical metallurgy, e.g., in studies of internal oxidation, case hardening, and dispersion hardening.

It should be borne in mind, however, that there are a number of factors which limit the stress–strain analysis of materials by the divergent beam method and these will now be discussed.

(1) The method in its present form is solely restricted to the study of single crystals having faces not less than 4 mm². It is quite possible, however, that in the future it can be extended to polycrystalline specimens if the following modifications in instrumentation are adopted: (a) construction of an x-ray tube with spot size of about 1 μ; (b) narrowing of the tip of the x-ray tube so as to reduce the instrumental obstruction to the x-rays diffracted by the specimen. If these requirements are fulfilled, the specimen may be brought closer to the x-ray source and grains approximately 250 μ in size can be studied.

(2) The crystal must exhibit in its undeformed state a fairly high degree of lattice perfection and must be free of surface distortions. The undeformed state is regarded as the reference state to which all measured strains, that is, $\Delta d/d$ values, are referred. The required degree of lattice perfection for the reference state is defined by the absence of those characteristics of the x-ray pattern discussed in Sec. 4.

If the strain distribution in the crystal becomes inhomogeneous and the pattern shows manifestations of broadening, kinking, and displacement of the lines, the strain analysis has to be augmented by a Fourier transform analysis of the line profile (Sec. 4). The divergent beam method offers, however, the great advantage that the individual (hkl) reflections of a form are not superposed as in the powder technique, which is the basis of current Fourier methods.

(3) More than six independent (hkl) reflections have to be analyzed.[1] Furthermore, to obtain a representative sampling of the strain ellipsoid the crystal must be studied in different directions. This necessitates irradiation of a number of different plane faces of the specimen.

(4) The smallest measurable strains for a particular (hkl) reflection must be larger than the experimental error defined by the corresponding $\bar{\sigma}_d$ value (Sec. 7).

ACKNOWLEDGMENT

The authors express their gratitude to Professor J. J. Slade for critical comments and stimulating discussions.

APPENDIX A

Least-Squares Determination of $y=mx+B$

The least-squares estimates of m_i, $i=1, 2$ and B_i, $i=1, 2$ are obtained by minimizing the sum of the squares of the deviations:

$$S=\sum_j (y_{ij}-m_i x_{ij}-B_i)^2, \qquad \begin{matrix} i=1, 2 \\ j=1, n_i, \end{matrix}$$

where n_i is the number of determinations for each line.

We have, using the expressions from the regression theory,[11,12]

$$m_i=\sum_j y_{ij}(x_{ij}-\bar{x}_i)/\sum(x_{ij}-\bar{x}_i)^2, \quad i=1, 2 \quad \text{(A1)}$$

$$B_i=\bar{y}_i-m_i\bar{x}_i, \qquad i=1, 2. \quad \text{(A2)}$$

The variance of estimate is given by

$$V_i(y/x)=\sum(y_{ij}-m_i x_{ij}-B_i)^2/(n-2), \quad i=1, 2, \quad \text{(A3)}$$

where m_j and B_j are given by (A1) and (A2), respectively, and the notation $V_i(y/x)$ stands for the variance of y given x, that is, the variance about the least-squares line.

The variance of the slope is given by

$$V(m_i)=V_i(y/x)/\sum_j (x_{ij}-\bar{x}_i)^2, \quad i=1, 2. \quad \text{(A4)}$$

d Spacing and its Standard Error

α and d are given by Eqs. (5) and (6). Knowing the standard error of the slopes m_1 and m_2 we can compute the standard error of the d spacing. In fact, we have

$$V(\alpha)=\frac{k^2}{4}\left[\frac{V(m_1)}{[1+(km_1)^2]^2}+\frac{V(m_2)}{[1+(km_2)^2]^2}\right] \quad \text{(A5)}$$

and

$$V(d)=(\lambda^2/4)(\sin^2\alpha/\cos^4\alpha)V(\alpha). \quad \text{(A6)}$$

The standard error of d is then

$$\sigma_d=[V(d)]^{\frac{1}{2}}. \quad \text{(A7)}$$

Weighted Least Squares

The relation between the lattice parameter a' and x,

[11] A. Hald, *Statistical Theory with Engineering Applications* (John Wiley & Sons, Inc., New York, 1952), Chap. 18.

[12] A. H. Bowker and G. J. Lieberman, *Engineering Statistics* (Prentice-Hall, Inc., Englewood Cliffs, New Jersey, 1959), Chap. IX.

Sec. 6, is given by

$$a' = a_0 + bx, \tag{A8}$$

where

$$x = \tfrac{1}{2}[(\cos^2\theta/\sin\theta) + \cos^2\theta/\theta].$$

Since the standard error of d and, therefore, of a' depends on the value of θ, a weight inversely proportional to the variance of d was assigned to the a' values.

This weight was defined as

$$w_i = [1/(\sigma_{d_i}{}^*)^2]/\sum(1/\sigma_{d_i}{}^*)^2, \tag{A9}$$

where

$$(\sigma_{d_i}{}^*)^2 = \sum_j [(d_{ij} - \bar{d}_i)^2/(n-1)] \tag{A10}$$

and $j = 1 \cdots n_1$, the number of d-spacing determinations for each Bragg angle θ and $i = 1 \cdots k$, the number of Bragg angles (see Fig. 6).

The values of a_0 and b are obtained by minimizing the sum of the squares of the deviations:

$$S = \sum_i n_i w_i (a_i' - a_0 - bx_i)^2.$$

Again, using the results from weighted least squares, we have

$$b = \sum n_i w_i a_i' (x_i - \bar{x})/\sum n_i w_i (x_i - \bar{x})^2 \tag{A11}$$

and

$$a_0 = \bar{a}' - b\bar{x}, \tag{A12}$$

where

$$\bar{a}' = \sum n_i a_i' w_i/\sum n_i w_i, \tag{A13}$$

$$\bar{x} = \sum n_i x_i w_i/\sum n_i w_i. \tag{A14}$$

The variance of estimate is given by

$$V(a'/x) = \sum n_i w_i (a_i' - a_0 - bx_i)^2/(n-2), \tag{A15}$$

where b and a_0 are given by (A11) and (A12), respectively.

The variance of b and a_0 are given by

$$V(b) = V(a'/x)/\sum n_i w_i (x_i - \bar{x})^2 \tag{A16}$$

$$V(a_0) = V(a'/x)[(1/n) + \bar{x}^2/\sum n_i w_i (x_i - \bar{x})^2]. \tag{A17}$$

The standard errors are then

$$\sigma_b = [V(b)]^{\frac{1}{2}}, \tag{A18}$$

$$\sigma_{a_0} = [V(a_0)]^{\frac{1}{2}}. \tag{A19}$$

APPENDIX B

Computation of d Spacings from Incomplete Ellipses

Referring to Fig. 1 it will be seen that

$$NP = (a+b)\cot(\theta+\beta) + b\cot(\theta-\beta)$$
$$= a\cot(\theta+\beta) + b[\cot(\theta+\beta) + \cot(\theta-\beta)] \tag{B1}$$

$$NR = b\cot(\theta+\beta) + (a+b)\cot(\theta-\beta)$$
$$= a\cot(\theta-\beta) + b[\cot(\theta+\beta) + \cot(\theta-\beta)]. \tag{B2}$$

Let $NR = t$, for brevity, and suppose that two patterns are superimposed on the same film by making two exposures and changing the distance a from the film to the target between the exposures. Then, for example, Eq. (B2) gives

$$t_1 = a_1\cot(\theta-\beta) + b[\cot(\theta+\beta) + \cot(\theta-\beta)], \tag{B3}$$

$$t_2 = a_2\cot(\theta-\beta) + b[\cot(\theta+\beta) + \cot(\theta-\beta)], \tag{B4}$$

where the subscripts refer to the film position.

Subtracting (B4) from (B3),

$$t_1 - t_2 = (a_1 - a_2)\cot(\theta-\beta) = c\cot(\theta-\beta)$$
$$\cot(\theta-\beta) = (t_1 - t_2)/c = \Delta/c. \tag{B5}$$

Here c is the distance through which the film has been shifted between exposures and $t_1 - t_2$ is the distance between corresponding ellipses measured on the film along their common major axis.

Let us now assume that the incident radiation consists of two components of wavelength λ_1 and λ_2, respectively, each giving rise to a pattern. We have then from (B5)

$$\theta_1 - \beta = \operatorname{arccot}(\Delta_1/c), \tag{B6}$$

$$\theta_2 - \beta = \operatorname{arccot}(\Delta_2/c), \tag{B7}$$

where the subscripts now refer to different wavelengths. Subtracting (B7) from (B6),

$$\theta_1 - \theta_2 = \operatorname{arccot}(\Delta_1/c) - \operatorname{arccot}(\Delta_2/c)$$
$$= \operatorname{arccot}[(c^2 + \Delta_1\Delta_2)/c(\Delta_1 - \Delta_2)] = \mu. \tag{B8}$$

Let

$$\lambda_1/\lambda_2 = \sin\theta_1/\sin\theta_2 = K,$$

then

$$\sin\theta_1 = \sin(\mu + \theta_2) = K\sin\theta_2. \tag{B9}$$

The second of Eq. (B9) gives finally,

$$\cot\theta_2 = (K - \cos\mu)/\sin\mu, \tag{B10}$$

where μ is given by (B8).

The last expression gives the value of the Bragg angle (and therefore of the interplanar spacing) of a given set of planes in terms of the known x-ray wavelengths, of the film shift between exposures c, and of two quantities Δ_1 and Δ_2 measured on the film (Figs. 1 and 5).

Equation (B10) may be written in a form which gives directly the d spacings, obviates the need for trigonometric tables, and is convenient for computation on a desk calculator. Using the identity $\sin\theta = (1+\cot^2\theta)^{-\frac{1}{2}}$ and the value of $\cot\theta_2$ given by (B10),

$$\lambda_2 2\sin\theta_2=(\lambda_2/2)(1+\cot^2\theta)^{\frac{1}{2}}$$
$$=(\lambda_2/2)\{1+[(K-\cos\mu)/\sin\mu]^2\}^{\frac{1}{2}}$$
$$=((\lambda_2^2/4)\{1+[(K/\sin\mu)-\cot\mu]^2\})^{\frac{1}{2}}. \quad \text{(B11)}$$

Using the trigonometric identity mentioned above and setting $\cot\mu=s$, the factor in brackets in the last member of (B11) can be written

$$1+[(K/\sin\mu)-\cot\mu]^2=(1+K^2)(1+s^2)-2Ks(1+s^2)^{\frac{1}{2}}.$$

Using this expression in (B11) we obtain finally,

$$d=[K'(1+s^2)-K''s(1+s^2)^{\frac{1}{2}}]^{\frac{1}{2}}$$

with

$$K'=(\lambda_1^2+\lambda_2^2)/4, \quad K''=\lambda_1\lambda_2/2,$$

and

$$s=\cot\mu=(c^2+\Delta_1\Delta_2)/c(\Delta_1-\Delta_2)$$

by Eq. (B8).

JOURNAL OF APPLIED PHYSICS VOLUME 35, NUMBER 11 NOVEMBER 1964

Stress-Strain Analysis of Single Cubic Crystals and Its Application to the Ordering of CuAu I. Paper II

J. J. Slade, S. Weissmann, K. Nakajima,* and M. Hirabayashi*
College of Engineering, Rutgers, The State University, New Brunswick, New Jersey
(Received 20 April 1964)

A stress–strain analysis of single cubic crystals is developed which utilizes the strain data supplied by the x-ray back-reflection divergent beam method. The principal strains and their directions are determined and from the principal strains and the known elastic constants the complete stress–strain configuration is obtained. Thus the maximum magnitude and the direction of the shearing strain on a given set of crystallographic planes are obtained and the set of planes on which the maximum value of the shearing maxima occurs is also determined. From a knowledge of the stress–strain configuration, the stored elastic energy of the crystal is deduced; it can be partitioned into two components, that due to shearing strains and that due to a mixture of normal and shearing strains.

The conditions under which the principal stress system coincides with the principal strain system are also investigated. Furthermore, a number is constructed that measures the distortion of the crystal in terms of the energy increments associated with the elastic constants.

The stress–strain analysis applied to the ordering of a CuAu crystal at 125°C corroborates quantitatively the qualitative results previously obtained by transmission electron microscopy. The dependence of stored elastic energy on annealing time is determined and it is shown that the first maximum and decline are associated with the maximum and decline of coherency strains set up between the ordered CuAu I nuclei and the disordered matrix. Upon increasing the annealing time, twinning occurs to relieve the tetragonality strains introduced by the ordered CuAu I domains. The second maximum is compounded by twinning on certain (110) planes and delayed ordering on other (110) planes of the matrix. The subsequent decline of the stored elastic energy is associated with twinning on all (110) planes. The shearing stress necessary to initiate microtwinning does not exceed 7×10^8 dyn/cm^2.

1. INTRODUCTION

STUDYING by means of transmission electron microscopy the ordering of CuAu I, Hirabayashi and Weissmann[1] have shown that at low-temperature annealing plate-like nuclei are formed which are coherent with the disordered matrix and parallel to the (101) planes. Upon prolonged annealing at low temperature or short annealing at elevated temperature, the accumulated coherency strains introduced by the tetragonality of the ordered CuAu I structure become relieved through twinning and the twin planes are also parallel to the (101) planes of the cubic matrix. It was impossible, however, to obtain by electron microscope techniques quantitative information as to what the distribution and magnitude of the strains were that led to the observed twinning during ordering. Yet such information is highly desirable if a detailed picture of the mechanism of ordering is to emerge.

The x-ray studies presented in this paper were undertaken to supplement the qualitative results of the electron microscope investigation by quantitative data. The interpretation of the quantitative results required an extension of the strain analysis[2] recently developed, which uses the strain data supplied by the x-ray back-reflection divergent beam method. Thus a complete stress–strain analysis was developed which describes the stress–strain configuration for the early ordering stages of CuAu I. It also enables one to study the changes in stored elastic energy and anisotropy of strain distribution as a function of ordering anneal. Since the developed stress–strain analysis of cubic crystals appears to have a more universal application than shown in the specific study of the ordering of

* Present address: Research Institute for Iron, Steel, and Other Metals, Tohoku University, Sendai, Japan.

[1] M. Hirabayashi and S. Weissmann, Acta Met. 10, 25 (1962).

[2] T. Imura, S. Weissmann, and J. J. Slade, Jr., Acta Cryst. 15, 786 (1962).